Submitted, accepted and published by
CHEMICAL ENGINEERING SCIENCE 122(2015)232–239
https://doi.org/10.1016/j.ces.2014.09.033

Mercury capture by a regenerable sorbent under oxycoal combustion conditions: effect of SO_2 and O_2 on capture efficiency.

C. Gómez-Giménez[a], D. Ballestero[b], R. Juan[a], B. Rubio[a] and M.T. Izquierdo[a]*

[a]Instituto de Carboquímica, ICB-CSIC. c/Miguel Luesma Castán, 4. 50018 Zaragoza, Spain.

[b]Universidad San Jorge. Autovía A23 Zaragoza-Huesca km 510. 50830 Villanueva de Gállego, Zaragoza. Spain.

*corresponding author: mizq@icb.csic.es

Abstract

The present study, evaluates an Au/C sorbent based on the direct reduction of a gold salt on a carbon coated structured cordierite monolith for mercury capture under oxyfiring conditions. Both mercury retention efficiency and mercury retention capacity were tested in a bench scale plant under different conditions. The influence of gas temperature (50º-150ºC) and gas composition (CO_2, N_2, SO_2, O_2) on sorbent performance for mercury capture is evaluated and discussed. The amount of mercury captured did not vary significantly with temperature under a CO_2 atmosphere. These results were compared with those obtained under N_2 atmosphere with no remarkable differences found between them. High retention efficiencies were obtained despite the small amount of gold used. The presence of SO_2 and O_2 in the flue gas led to mercury oxidation that seemed to be mainly promoted by SO_2 under the presence of the Au-sorbent.

Keywords: Regenerable sorbent**;** Hg capture; Au nanoparticles; Oxycombustion

1. Introduction

Greenhouse gas emissions are currently an issue of international concern owing to their serious long term consequences. Carbon dioxide is the largest contributor to the greenhouse effect and the energy sector accounts for more than 40% of global CO_2 emissions, being coal combustion the major source of these emissions worldwide (Statistics., 2012). Carbon capture and storage (CCS) technology is therefore a crucial tool for decarbonizing the global economy.

Oxy-fuel combustion is one of the promising technologies used to capture CO_2 from power plants (Wilcox, 2012). In this system, pure oxygen alone is introduced and part of the flue gas, mainly composed of CO_2 and H_2O, is recirculated to reduce boiler temperature. Flue gas impurities such as N_2, O_2, NO_x, SO_x, and heavy metals can be present and these need to be removed before CO_2 capture and compression unit. One pollutant which has to be taken into account is mercury, because it forms an amalgam with aluminum that causes corrosion in heat exchangers in the CO_2 processing unit (Bessone, 2006; Craig, 1992). Moreover, mercury concentration is higher in flue gas under oxy-firing conditions. Therefore, effective mercury removal in oxy-combustion is not only related to environmental issues, but it is also a technical specification.

The chemical forms of emitted mercury can be classified as elemental mercury (Hg^0), oxidized mercury (Hg^{2+}), and mercury in association with particulate matter (Hg_p). At temperatures greater than 1200ºC, mercury exits the boiler primarily in elemental form. As the flue gas cools, physical and chemical transformation mechanisms may control mercury speciation. Hg oxidation mainly depends on the concentration of halogen species present in coal, coal type, and specific equipment configurations (Wilcox et al., 2012).

The main mechanism currently available for reducing Hg emissions is the use of air pollution control devices designed to remove NO_x, SO_x, and fly ashes from flue gas. Selective Catalytic Reduction (SCR) system promotes the oxidation of elemental mercury (Rallo et al., 2012). Additionally, mercury adsorbed on fly ashes is captured in the particulate matter control devices and removed by electrostatic precipitators (ESP) and fabric filters (FF). Finally, oxidized mercury is removed in wet flue gas desulfurization systems (WFGD) owing to the high solubility of Hg^{2+} in water. Elemental mercury is almost insoluble in water and is difficult to remove from flue gas, which makes the development of mercury-specific control technologies necessary.

The only proven technology for mercury capture is the injection of activated carbon (ACI) into the flue gas ductwork. Mercury bound with the activated carbon is removed in particulate collection devices downstream. The main drawback of ACI technology is the high carbon to mercury ratio needed to achieve high retention efficiency. As a result, a large amount of residue is generated and removed with fly ashes. This leads to the loss of fly ash marketability. Pulverized-coal power plants working under oxy-firing conditions, such as Schwarze Pumpe (Germany), have an adsorbing tower of S-doped activated carbon positioned before the CO_2 processing units. However, the spent activated carbon must be treated as a toxic residue.

Fixed structures for mercury capture are being developed in order to resolve this drawback. Furthermore, these fixed structures can be designed as regenerable sorbents for mercury capture. They can be coated with noble metals because of amalgamation capacity of mercury with them. Since the early 1970s, gold has been used in some devices to determine mercury content (Anderson et al., 1971).

The use of gold-based sorbents for mercury capture has the advantage that they can be regenerated. The regenerability of these sorbents would enable the recovery of desorbed mercury for commercial recycling or disposal. The amount of Au required can be reduced by using Au nanoparticles in order to maximize the specific surface area of Au.

Gold particle size is very important to determine its reactivity since nanometric gold has been found to have catalytic properties (Guan & Hensen, 2009; Haiss et al., 2007; Jeon & Lee, 2011; Rodriguez et al., 2003). Combustion environment plays an important role in mercury capture since oxidized mercury cannot be retained by amalgamation. Hg can be oxidized in the presence of Au nanoparticles under SO_2 and O_2 atmosphere (Biener et al., 2005), which would lead to mercury capture inhibition (Edge et al., 2011).

The regenerability of a sorbent based on gold nanoparticles supported on structured carbon monoliths was tested throughout several capture-regeneration cycles in previous work (Ballestero et al., 2013) using the same methodology for gold deposition but different conditions for the deposition. Consequently, the aim of this work was to capture mercury by means of the sorbent under a CO_2 rich atmosphere, compared with previous tests under N_2 atmosphere. The sorbent was developed for placement before or after the flue-gas desulfurization system, and was therefore evaluated under different temperatures in the range of 50ºC-150ºC. Finally, we studied the effect of SO_2 and O_2 on the sorbent as well as on mercury capture efficiency.

2. Experimental

2.1. Preparation of sorbent

A cordierite honeycomb structure (from Corning Inc.) was used as the starting material for the preparation of supports owing to its low pressure drop, high surface area to volume ratio, and high thermal and mechanical stability.

The cordierite structure was impregnated with a phenolic resin (Novolak type delivered by Ilarduya, from Hüttenes Albertus group), which was allowed to soak into it. The resin was thermally cured at 150ºC for 1h. Carbonization was subsequently carried out at 700ºC for 1h under an Ar flow. The resin impregnation, curing, and carbonization process were repeated twice to obtain a homogeneous carbon surface. This carbon support had square channels with a density of 33 cells/cm^2 and a length of 15 mm.

The method for gold deposition involved the direct reduction of gold salt ($HAuCl_4 \cdot 3H_2O$) by the actual carbon support surface without the addition of reducing or protective chemicals. The support was immersed in a 0.127 mM aqueous gold salt solution. A stirring rate of 150 rpm was used in order to force the solution to pass through the channels, and the reaction time was 20 minutes, 10 minutes for each stir flow direction. This procedure was tested by preparing several samples of the sorbent in order to check reproducibility in terms of gold content, gold distribution and gold average particle size.

After gold deposition, the samples of sorbent were subjected to Reducing Thermal Treatment (RTT) at 300ºC for 1 hour in a flow containing 4% H_2 in N_2.

2.2. Characterization of sorbent

After gold deposition, the sorbent was characterized by different techniques. The bulk gold content of the sorbent was determined by Inductively Coupled Plasma Optical Emission Spectroscopy (ICP-OES) with a Jobin Ybon 2000 equipment. The sample was previously digested with *aqua regia*.

Scanning Electron Microscopy with Energy Dispersive X-ray Spectroscopy (SEM-EDX) analysis was conducted using a Hitachi S-3400 N microscope equipped with a Röntec XFlash Si(Li) EDX detector to obtain the surface gold content (detailed procedure is given in Ballestero et al., 2014). Gold nanoparticle size distribution was obtained by Scanning Electron Microscopy with Field Emission (FE-SEM) using a Carl Zeiss MERLIN microscope equipped with an In-Lens detector. The images were analyzed by Image J, free software for image analysis (detailed procedure given in Ballestero et al., 2014).

X-ray diffraction (XRD) was used to obtain information regarding the crystalline structure of the gold. XRD diffractograms were collected by a Bruker D8 Advance X-ray powder diffractometer equipped with an X-ray source with a Cu anode working at 40 kV and 40 mA, a Göbel mirror, and a scintillation detector. The diffraction pattern was obtained over the 2θº range of 35º-80º, with a step-size of 0.05°, and at grazing incidence.

The influence of O_2 and/or SO_2 on the sorbent, in the presence and absence of mercury, was studied by Xray Photoelectronic Spectroscopy (XPS). XPS analyses were performed with an ESCAPlus Omicron spectrometer equipped with a non-monochromatized MgKα radiation source (1253.6 eV). The samples were introduced into the analysis chamber where the vacuum was lower than $5 \cdot 10^{-9}$ torr. The hemispherical electron energy analyzer was operated at pass energy of 50 eV for surveys, and 20 eV for high-resolution spectra. The energy scale was calibrated by referencing the C1s peak to 284.5 eV. CASA software was used to process the XPS data.

2.3. Mercury capture tests

A bench-scale plant was specifically designed and built to test the sorbent. The experimental installation is shown schematically in Fig. 1. A battery of flow meters was used to control the composition and flow-rate of the simulated flue gas. A certified Dynacal Hg^0 permeation device with an accuracy of ±0.01ºC was used to generate a constant feed of Hg^0. The resulting gas mixture was sent to the quartz reactor tube, with an internal diameter of 16 mm, where the sorbent was fitted between two ceramic pieces. A furnace surrounding the reactor was used to control the temperature. An on-line elemental mercury analyzer (VM3000) continuously monitored Hg^0 evolution downstream of the sorbent. The reactor was provided with a bypass which allows to measure the Hg concentration before starting an experiment and after finishing the experiment. At the end of the line, a modified Ontario Hydro Method (OHM) was placed to capture the oxidized mercury (Curtis & Eagleson, 1995). This system was composed of five flasks. Two empty impingers were placed in first and last position. The other three were filled with 100 mL of KCl 1M. All the flasks were partially immersed in a cold bath at 0°C. At certain times, the complete tail-end train of flasks was placed in order to verify the proper operation of the plant. In this case, two impinger groups were used to trap oxidized and elemental Hg. The first group of impingers contained a solution of KCl 1M to trap Hg^{2+} and the second group contained a solution of 4% $KMnO_4$– 10% H_2SO_4 to trap Hg^0. The fittings and tubings, where mercury was present, were made of Teflon to prevent possible mercury attack on the steel.

Hg breakthrough curves were obtained at a ratio of W_{Au}/Q of 4×10^{-5} g h l^{-1}, where W_{Au} was the weight of Au used in each experiment (about 0.4 mg) and Q was the total gas flow (0.25 l h^{-1} at STP), at temperatures ranging from 50 to 150ºC and at Hg inlet concentration of 100 μg/m^3 in N_2 and CO_2 atmospheres. Some

experiments were performed two or three times under the same operational conditions in order to test reproducibility. The amount of Hg captured in the sorbent and the retention efficiency achieved were measured at 20% and 80% saturation. The total amount of Hg^0 retained was calculated by integration of the breakthrough curve. Hg retention efficiency was calculated as the ratio between the amount of Hg retained by the sorbent at each percentage of saturation and the total amount of Hg fed during this time. A baseline test with the support (no Au) was carried also out in order to determine mercury adsorption owing to the carbon material. This value was <0.30 μg Hg/g support and is subtracted from the mercury capture values reached by the sorbent.

After a number of experiments, the exhausted samples of sorbent were analyzed by an Advanced Mercury Analyzer (AMA from LECO) to determine the mercury captured on them. The total amount of sample used for the mercury capture experiment was crushed and aliquots were analyzed in the AMA. These results were compared with those obtained from the mercury breakthrough curves.

3. Results and Discussion

3.1. Sorbent characterization

The bulk gold content of the sorbent that was determined by ICP-OES was 0.11 wt%. The surface gold content obtained by SEM-EDX was 2.5 wt%. It could therefore be assumed that the gold was mainly located on the support surface.

The gold particle size distribution was obtained by FE-SEM, for which several micrographs were taken. The established method for analyzing the sorbent was based on taking seven images per channel and two channels per monolith, one inner and another outer, and later analyzing them by Image J. The micrographs showed

that gold particles were homogeneously deposited on the support surface (Fig. 2). The particle size distribution from Image J analysis is shown in Fig. 3. The average particle size obtained was 61 nm.

Fig. 4 shows the XRD pattern of the sorbent. According to the Joint Committee on Powder Diffraction Standards database, the XRD pattern shows the typical peaks expected for Fm-3m (225) gold. The main diffraction gold peaks in the sample are situated at 38.25º, 44.45º, 64.75º, and 77.65º, which correspond to gold (111), (200), (220) and (311) planes, respectively. Small peaks not identified in Fig. 4 correspond to cordierite phases. As can be seen, the principal peak is Au (111). The plane corresponding to this peak is the most active one of all and enhances the amalgamation process (Kobiela et al., 2003; Lim & Wilcox, 2013; Lim et al., 2012). The explanation of this lies in the fact that the (111) plane corresponds to the highest atomic density in fcc structures, which makes this orientation the most stable one. Whole pattern decomposition was performed using the Le Bail method with pseudo-Voigt approach in order to obtain crystallite size. The volume weighted column height (LVol-IB) was taken to obtain the average crystallite size, which was 24 nm. This value was lower than that obtained from the analysis of particle size. As can be seen in Figure 2, the sphericity of the particles was low, indicating that the nearest particles could agglomerate during deposition and further thermal treatment, producing larger particles.

These Au nanoparticles were mainly in the elemental state as the RTT enhanced their presence as Au^0. XPS spectra obtained both before and after RTT were very similar to those obtained in a previous work in which another type of carbon support was used (Ballestero et al., 2013). All these spectra confirm that, after RTT,

the amount of oxidized gold decreases. As mercury can only amalgamate with Au^0, the reducing treatment increases the number of active sites for mercury capture.

3.2. Mercury retention tests

Both the Hg capture capacity by gold content of sorbent and the Hg retention efficiency obtained at temperatures ranging from 50º to 150 ºC and with a mercury inlet concentration of 100 µg/m^3, are depicted in Fig. 5. As can be seen, the mercury capture efficiency at 20% breakthrough was higher than that achieved at 80% for all the studied temperatures. However, this efficiency decreased slightly with temperature. This can be attributed to the low temperature needed to regenerate the sorbent, as previously studied (Ballestero et al., 2013). At 80% breakthrough, mercury capture efficiency was around 60 per cent.

At 120ºC, the results obtained when the experiments were carried out under a N_2 were very similar to those obtained when the experiments were carried out under a CO_2 atmosphere. Hence, in the absence of any other compound, the sorbent was able to present the same behavior under oxy-firing conditions as that found under air-firing conditions.

In order to study the thermal stability for particle size, we tested the sorbent under 300ºC (the same temperature than for RTT and higher than previously tested for regeneration) during one month. In a real situation, the sorbent would be exposed approximately the same time for capture and for regeneration; this represents two months of real operation of the sorbent. The sample was removed from the reactor periodically and images from FE-SEM were taken, following the same procedure described in the experimental section. Image J was used to analyze the images to obtain gold particle size and surface area covered by the particles at

different periods of time. The results of this test are depicted in Fig. 6. As can be seen, the sorbent is stable for the 30 days test.

In addition to the temperature effect in the range of 50ºC-150ºC, it is important to understand the influence of gas composition on the Hg captured by the sorbent.

Two types of experiments were conducted in order to study the influence of O_2 and SO_2 on the sorbent performance.

One set of experiments was designed to evaluate changes in the sorbent in the presence of O_2 and/or SO_2 in the absence of mercury. A second set of experiments was conducted to evaluate the sorbent after mercury capture under different atmospheres in the bench-scale installation. Exhausted sorbent was also analyzed by XPS after the experiments.

The idea behind the first set of experiments was to know whether the sorbent could be modified by different gases when mercury was not present, because nanometric Au has catalytic properties. These compounds were studied because SO_2 is believed to enhance homogeneous Hg oxidation (Biener et al., 2005) and therefore inhibit mercury capture (Edge et al., 2011), and because a higher concentration of O_2 could cause an increment in SO_3 concentration.

The supported Au surface may contain enough defect sites to enhance gold catalytic activity for O_2 and SO_2 dissociation. As a result of the former, dissociated atoms could occupy active surface sites because of the greater concentration of these species in comparison with Hg^0 in the flue gas environment. SO_2 was present in the flue gas at ppm levels and Hg^0 at ppb level.

The study was carried out with fresh sorbent. First, an XPS spectrum of the fresh sorbent was recorded, and C1s, O1s, and Au4f regions were carefully studied. The sorbent subsequently underwent in situ treatment with different gas atmospheres for

2 hours at 120ºC. A new spectrum of the treated sample was then obtained. The studied atmospheres were 5% O_2 in CO_2, 2500 ppmv SO_2 in CO_2 and 2500 ppmv SO_2, 5% O_2 and the remainder CO_2. In the case of SO_2-containing atmospheres, the S2p region was also studied. The results of curve fitting of the Au region as well as the region quantification for all the experiments are summarized in Table 1.

Fig. 7 illustrates the Au4f region with two well-resolved peaks: $Au4f_{5/2}$ and $Au4f_{7/2}$. This figure compares the spectra obtained before and after each flow gas treatment. As can be seen in Table 1, the Au4f curve fitting of the spectra, obtained before in situ treatment, show two $Au4f_{7/2}$ components centered at 84 and 85.2 eV, and another two $Au4f_{5/2}$ components centered at 87.7 and 88.8 eV. According to the literature (Bulushev et al., 2004; Casaletto et al., 2006; Thome et al., 1998), the signals at binding energies of 84 and 87.7 eV are assigned to metallic gold, while the ones obtained at 85.2 and 88.8 eV correspond to ionic gold species $Au^{\delta+}$. As shown in Table 1, the gold nanoparticles were mainly elemental gold.

When a sorbent was treated with O_2, there was no Au4f peak displacement and C1s and O1s peaks remained almost unaltered. However, a small increase in the $Au^{\delta+}$ contribution could be found (Table 1), although this was not enough to alter the Au4f peak. The spectra obtained after SO_2 treatment, with or without O_2, were very similar. In both cases there was a slight shift in Au4f peak to higher binding energies, which can be followed in Fig. 7, indicating a higher contribution of Au oxidized species. The C1s peak remained unaltered after treatment with SO_2 containing atmospheres and there was a slight increase in oxygen contribution. Sulfur was detectable by XPS in both SO_2-containing atmospheres. The only difference between flowing O_2 with it or not was S quantification. S could only be quantified in the first case, giving a value of 0.5% (atomic percentage).

In view of these results, it can be hypothesized that there is one possible mechanism for sulfur deposition on Au surface involving SO_2 and SO_3, since, SO_2 can be oxidized to form SO_3 at temperatures lower than 1000ºC, (Sellers & Shustorovich, 1997). At temperatures below 500ºC, SO_3 can be oxidized to form sulfuric acid, which can modify the surface of gold. Moreover, Au nanoparticles are catalysts for SO_2 decomposition, and elemental sulfur can be deposited on the sorbent surface (Biener et al., 2005; Rodriguez et al., 2003). Thus, the former shows that an understanding of SO_2 adsorption on Au is a necessary step toward the elucidation of Hg oxidation on Au.

The influence of gas composition was also studied in the bench-scale plant. Hg breakthrough curves were obtained at 120ºC and Hg inlet concentration of 100 $\mu g/m^3$. Samples of sorbent were tested under four different atmospheres similar to those simulated in the in situ XPS study. The experimental results are presented as breakthrough curves in Fig. 8, where C_0 refers to initial mercury concentration and C refers to mercury concentration at each time. Although it could seem that breakthrough curves level off around C/C_0 0.8, long-term experiments (two days) show that breakthrough curves reach asymptotically the initial Hg concentration. The amount of mercury captured was obtained by integration of the breakthrough curves, and the results are reported in Table 2, corrected for support baseline. In view of the results, it seems that the presence of sulfur dioxide enhances mercury capture. To verify this point, previously tested exhausted samples of sorbent were analyzed by AMA in order to know how much mercury had been really captured. In the case of the presence of SO_2, concentrations obtained by AMA were different from those obtained from breakthrough curves, as can be observed in Table 3 (values of amount of mercury captured were corrected for support baseline).

The explanation for this is that the breakthrough curves were obtained by using an elemental mercury analyzer, which does not detect oxidized mercury. Consequently, the reliable amount of mercury captured by the sorbent is that shown in the first column of Table 3, which was measured directly on the sorbent by AMA device.

The analysis of the impinger solution indicates that oxidized mercury is generated when sulfur dioxide is present in the flue gas, as can be observed in Table 3. SO_2 promotes mercury oxidation and, therefore, reduces the effectiveness of the capture, because only elemental mercury can amalgamate with gold. Also, mercury capture decreases when oxygen is present. One reason may be that oxygen can oxidize the gold surface, which therefore decreases the number of active sites for Hg capture. Finally, when the flow contains both O_2 and SO_2, mercury oxidation is greater, as can be deduced from Table 3. This fact would suggest that oxygen has an important effect on mercury oxidation in the presence of Au. Oxygen modifies gold nanoparticles and oxygen can react with sulfur deposited on the sorbent. So, in this case, when oxygen is present in the gas, the amount of sulfur deposited on the sorbent is increased and it can be quantified. These hypotheses are in agreement with in-situ XPS results. However, it cannot be concluded where the S is deposited either over Au nanoparticles or the support.

To provide further details, exhausted sorbent were analyzed by XPS after the Hg capture experiments under the different atmospheres after around reaction times of 20 h. The Au4f spectra are represented in Fig. 9. The results of curve fitting of the Au4f region can be found in Table 4. It was observed that Au4f peaks displacement took place when the gas stream was composed of O_2, CO_2, and mercury. This displacement corresponded to Hg amalgamation, as had been observed previously

(Ballestero et al., 2013; Thome et al., 1998). Moreover, the $Au^{\delta+}$ contribution increased, as can be deduced from Table 4, according to the results found when analyzing in-situ XPS experiments. However, the C1s and O1s peaks remained almost unaltered, as was also found when conducting in situ XPS experiments. In this situation the Hg/Au ratio was 0.04. When the flue gases were composed of SO_2, CO_2, and mercury, the spectrum obtained also showed a Au4f peak displacement resulting from the amalgamation, as previously explained. In addition, the $Au^{\delta+}$ contribution was increased, according to the results of curvefitting reported in Table 4, the C1s peak remained almost unaltered, the O1s peak underwent a slight increase, and sulfur was detectable but not quantified. Also, the ratio Hg/Au was 0.04. Finally, when the flue gases were composed of SO_2, O_2, CO_2, and mercury, the spectrum obtained showed a Au4f peaks displacement of 0.1 eV to a more oxidized state, the C1s peak remained almost unaltered, and the O1s peak again underwent a slight increase. In this case, sulfur was detectable and quantified with a value of almost 1% (atomic percentage). The results obtained when SO_2 was present in the flue gas agreed with the results found when using in-situ XPS experiments.

It is worth noting that although mercury oxidation is a negative consequence for mercury retention by the sorbent, if the sorbent is placed before the FGD system, oxidized mercury can be removed inside this system. Furthermore, if the sorbent is placed after the FGD system, SO_2 concentration in the flue gas would be low and the sorbent would not be overly affected by this sulfur compound. Even if the FGD system were able to remove all the SO_2, this compound would not be in the flue gas and the sorbent would not be altered by it.

4. Conclusions

A structured Au/C sorbent for Hg capture based on the direct reduction of an Au salt by the actual carbonaceous support surface without the addition of reducing or protective chemicals was developed and tested for mercury capture.

High Hg retention efficiency can be achieved using this sorbent under a CO_2 atmosphere. As the amount of Hg captured does not vary significantly with temperature (50º-150ºC), the use of this sorbent is possible in different positions in power plants working under oxy-firing conditions.

The presence of SO_2 in the flue gas leads to Hg oxidation when gold nanoparticles are present. It can also be concluded that elemental sulfur is deposited on the sorbent surface since gold nanoparticles are catalysts for SO_2 decomposition.

In view of the aforementioned findings, this sorbent can be used upstream of FGD, because oxidized Hg will be retained in the FGD unit, or downstream of FGD, because no Hg oxidation or very low Hg oxidation is expected in the absence of SO_2 or when concentration is low,.

5. Acknowledgements

The financial support from Spanish Ministry of Science and Innovation and European Regional Developments Funds (ref: ENE2011-23412) is duly recognized. C. Gomez-Giménez thanks CSIC and European Regional Developments Funds for the grant received under the JAE program.

6. References

Anderson, D.H., Evans, J.H., Murphy, J.J., White, W.W., 1971. Determination of mercury by a combustion technique using gold as a collector. Anal. Chem. 43, 1511-1512.

Ballestero, D., Gómez-Giménez, C., García-Díez, E., Juan, R., Rubio, B., Izquierdo, M.T., 2013. Influence of temperature and regeneration cycles on Hg capture and efficiency by structured Au/C regenerable sorbents. J. Hazar. Mat. 260, 247-254.

Ballestero, D., Juan, R., Gómez-Giménez, C., García-Díez, E., Ruiz, C., Rubio, B., Izquierdo, M.T., 2014. Novel methodology for gold nanoparticles deposition on carbon monolith supports. Colloid Surf. A-Physicochem. Eng. Asp. 441, 91-100.

Bessone, J.B. 2006. The activation of aluminium by mercury ions in non-aggressive media. Corros. Sci. 48, 4243-4256.
Biener, M.M., Biener, J., Friend, C.M., 2005. Revisiting the S-Au(111) interaction: Static or dynamic? Langmuir 21, 1668-1671.
Bulushev, D.A., Yuranov, I., Suvorova, E.I., Buffat, P.A., Kiwi-Minsker, L., 2004. Highly dispersed gold on activated carbon fibers for low-temperature CO oxidation. J. Catal., 224, 8-17.
Casaletto, M.P., Longo, A., Martorana, A., Prestianni, A., Venezia, A.M., 2006. XPS study of supported gold catalysts: the role of Au^0 and $Au^{+\delta}$ species as active sites. Surf. Interf. Anal. 38, 215-218.
Craig, H.L., 1992. Detecting mercury amalgamation of aluminium by measuring potential difference between the aluminium surface and a reference electrode. M.O. Corporation. Patent US5171692-A.
Curtis, K., Eagleson, K., 1995. Speciation of mercury emissions from Ontario Hydro's coal-fired generating stations. Report No. A-F-95-22-Con. Ontario Hydro Technologies.
Edge, P., Gharebaghi, M., Irons, R., Porter, R., Porter, R.T.J., Pourkashanian, M., Smith, D., Stephenson, P., Williams, A., 2011. Combustion modelling opportunities and challenges for oxy-coal carbon capture technology. Chem. Eng. Res. Des. 89, 1470-1493.
Guan, Y.J., Hensen, E.J.M., 2009. Ethanol dehydrogenation by gold catalysts: The effect of the gold particle size and the presence of oxygen. Appl. Catal. A-Gen. 361, 49-56.
Haiss, W., Thanh, N.T.K., Aveyard, J., Fernig, D.G., 2007. Determination of size and concentration of gold nanoparticles from UV-Vis spectra. Anal.Chem. 79, 4215-4221.
Jeon, K.J., Lee, Z., 2011. Size-dependent interaction of Au nanoparticles and graphene sheet. Chem. Com. 47, 3610-3612.
Kobiela, T., Nowakowski, B., Dus, R., 2003. The influence of gas phase composition on the process of Au-Hg amalgam formation. Appl.Surf. Sci. 206, 78-89.
Lim, D.-H., Wilcox, J., 2013. Heterogeneous Mercury Oxidation on Au(111) from First Principles. Environ. Sci. Technol. 47, 8515-8522.
Lim, D.H., Aboud, S., Wilcox, J. 2012. Investigation of Adsorption Behavior of Mercury on Au(111) from First Principles. Environ. Sci. Technol. 46, 7260-7266.
Rallo, M., Heidel, B., Brechtel, K., Maroto-Valer, M.M., 2012. Effect of SCR operation variables on mercury speciation. Chem. Eng. J. 198, 87-94.
Rodriguez, J.A., Perez, M., Jirsak, T., Evans, J., Hrbek, J., Gonzalez, L., 2003. Activation of Au nanoparticles on oxide surfaces: reaction of SO_2 with Au/MgO(100). Chem. Phys. Lett. 378, 526-532.
Sellers, H., Shustorovich, E. 1997. Chemistry of sulfur oxides on transition metal surfaces: BOC-MP analysis. J. Mol. Catal. A-Chem. 119, 367-375.
Statistics, 2013. CO_2 emissions from fuel combustion - Highlights, International Energy Agency, IEA, Paris.
Thome, J., Himmelhaus, M., Zharnikov, M., Grunze, M., 1998. Increased lateral density in alkanethiolate films on gold by mercury adsorption. Langmuir, 14, 7435-7449.
Wilcox, J., 2012. Carbon Capture. Springer, New York.
Wilcox, J., Rupp, E., Ying, S.C., Lim, D.-H., Negreira, A.S., Kirchofer, A., Feng, F., Lee, K., 2012. Mercury adsorption and oxidation in coal combustion and gasification processes. Int. J. Coal Geol. 90, 4-20.

Figure captions

Fig. 1. Experimental installation for mercury capture tests.

Fig. 2. FE-SEM micrographs of the sorbent at different magnification.

Fig. 3. Particle size distribution from Image J analysis.

Fig. 4. XRD pattern of sorbent.

Fig. 5. Hg retention capacity and Hg retention efficiency at different temperatures and different atmospheres: (◆) 20 % breakthrough under an O_2/CO_2 atmosphere; (■) 80 % breakthrough under an O_2/CO_2 atmosphere; (▲) 20 % breakthrough under an O_2/N_2 atmosphere; (●) 80 % breakthrough under anO_2/N_2 atmosphere.

Fig. 6. Thermal stability at 300ºC for gold particle size and surface area covered by gold nanoparticles.

Fig. 7. XPS spectra of the Au4f region, before and after in situ XPS gas treatment and analysis, without the presence of Hg: (1) Before treatment with O_2; (2) After treatment with O_2; (3) Before treatment with SO_2; (4) After treatment with SO_2; (5) Before treatment with O_2 and SO_2; (6) After treatment with O_2 and SO_2;

Fig. 8. Hg breakthrough curves for sorbent tested under different atmospheres: (1) CO_2; (2) O_2+CO_2; (3) SO_2+CO_2; (4) O_2+SO_2+CO_2.

Fig. 9. XPS spectra of the Au4f region for sorbent tested in the bench scale plant under different atmospheres: (1) CO_2+Hg; (2) O_2+CO_2 +Hg; (3) SO_2+CO_2+Hg; (4) O_2+SO_2+CO_2+Hg.

Table 1. Relative surface distribution of gold species and chemical composition of sorbent tested in the in situ XPS study without the presence of Hg in the experiments.

Test conditions	BE (eV) and area of the peak (%)				C_{XPS} (%)	O_{XPS} (%)	Au_{XPS} (%)
	Au^0		$Au^{\delta+}$				
O_2/CO_2 before	84.0 (51.9)	87.7 (39.5)	85.2 (5.7)	88.8 (2.8)	86.6	6.9	6.5
O_2/CO_2 after	84.0 (51.0)	87.7 (38.5)	85.1 (6.9)	88.8 (3.4)	86.3	7.0	6.7
SO_2/CO_2 before	84.0 (51.3)	87.7 (38.6)	85.2 (6.2)	88.8 (3.2)	84.9	7.6	7.5
SO_2/CO_2 after*	84.1 (50.1)	87.8 (37.7)	85.2 (7.7)	88.9 (4.5)	84.4	8.0	7.6
$O_2/ SO_2/CO_2$ before	84.0 (50.9)	87.7 (38.5)	85.2 (6.8)	88.8 (3.5)	84.0	8.1	7.9
$O_2/ SO_2/CO_2$ after**	84.2 (48.8)	87.9 (38.0)	85.4 (8.5)	88.9 (4.7)	83.4	8.8	7.3

Binding energies (B.E.) are expressed in eV. Areas of the peak values are given in parentheses and are expressed as a percentage of the total area of the Au4f peak. C, O and Au elemental concentrations are presented as atomic percentage.

*S detectable, difficult to quantify

**0.5 at % S

Table 2. Total amount of Hg captured (from integration of the Hg breakthrough curves when different atmospheres were simulated).

Test conditions	Hg captured* (µg Hg/g sorbent)
Hg-CO_2	34.7
Hg-5% O_2-CO_2	33.5
Hg-2500 ppmv SO_2-CO_2	38.7
Hg-5% O_2-2500 ppmv SO_2-CO_2	37.3

*corrected for support baseline

Table 3. Amount of elemental mercury captured and amount of oxidized mercury trapped in the impinge solutions under different gas atmospheres determined by AMA (per g of sorbent)*.

Test conditions	µg Hg^0/g in exhausted sorbent	µg Hg^{2+}/g from impinger**	Total Hg (µg Hg^0+Hg^{2+}/g)
Hg-CO_2	33.01	0	33.01
Hg-5% O_2-CO_2	32.16	0	32.16
Hg-2500 ppmv SO_2-CO_2	27.83	5.58	33.41
Hg-5% O_2-2500 ppmv SO_2-CO_2	26.88	7.92	34.80

*corrected for support baseline

**referred to sorbent mass

Table 4. Relative surface distribution of gold species and chemical composition of exhausted sorbent analyzed by XPS after testing in the bench-scale installation.

Test conditions	BE (eV) and area of the peak (%)				C_{XPS} (at%)	O_{XPS} (at%)	Au_{XPS} (at%)	Hg_{XPS} (at%)
	Au^0		$Au^{\delta+}$					
CO_2	84.1 (50.6)	87.8 (39.2)	85.1 (6.6)	88.8 (3.5)	85.1	9.9	4.8	0.22
CO_2+O_2	84.1 (49.1)	87.8 (36.3)	85.1 (10.4)	88.8 (4.2)	84.9	10.3	4.6	0.20
CO_2+SO_2*	84.1 (47.1)	87.8 (37.3)	85.0 (11.1)	88.7 (4.5)	83.1	11.0	5.5	0.21
CO_2+O_2+SO_2**	84.2 (41.1)	87.8 (38.0)	84.9 (14.8)	88.6 (6.1)	81.6	12.1	5.2	0.14

Binding energies (B.E.) are expressed in eV. Areas of the peak values are given in parentheses and are expressed as a percentage of the total area of the Au4f peak. C, O, Au and Hg elemental concentrations are presented as atomic percentage.

*0.2 at % S

**0.9 at % S (oxidized species of S)

Figure 1

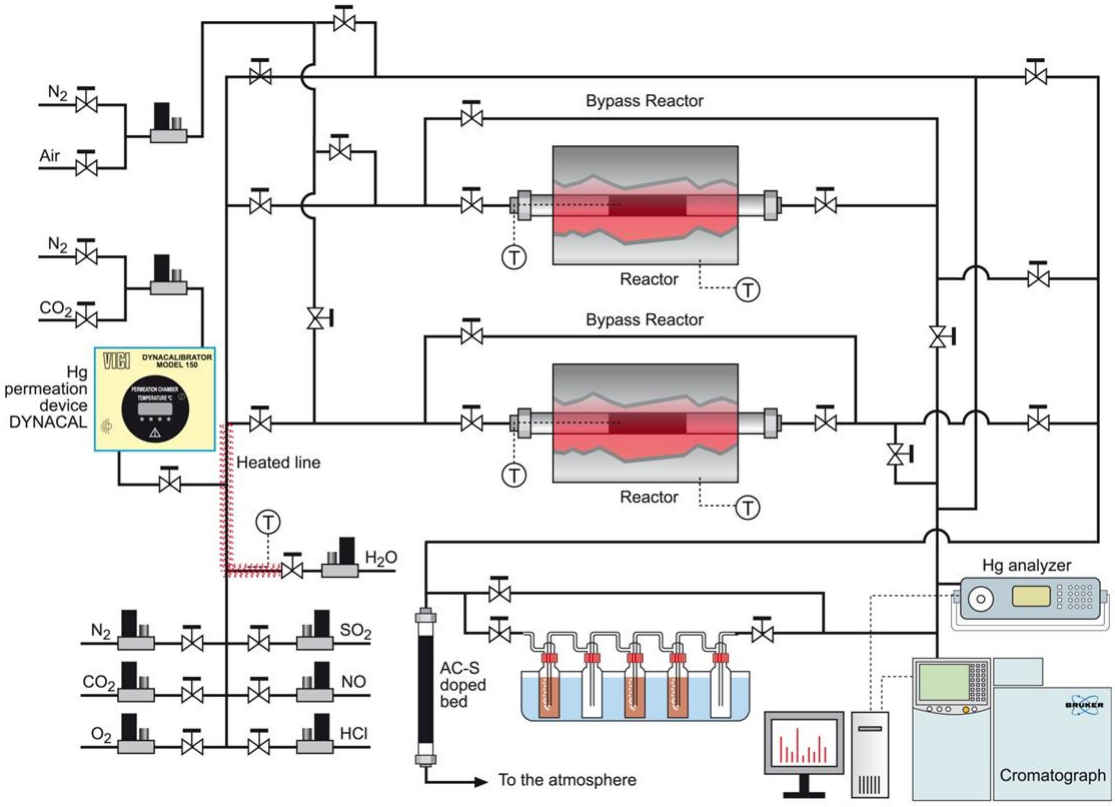
N2
Air
N2
CO2
Hg permeation device DYNACAL
DYNACALIBRATOR MODEL 150
Heated line
H2O
N2
CO2
O2
SO2
NO
HCl
Bypass Reactor
Reactor
Bypass Reactor
Reactor
Hg analyzer
AC-S doped bed
To the atmosphere
Cromatograph

Figure 2

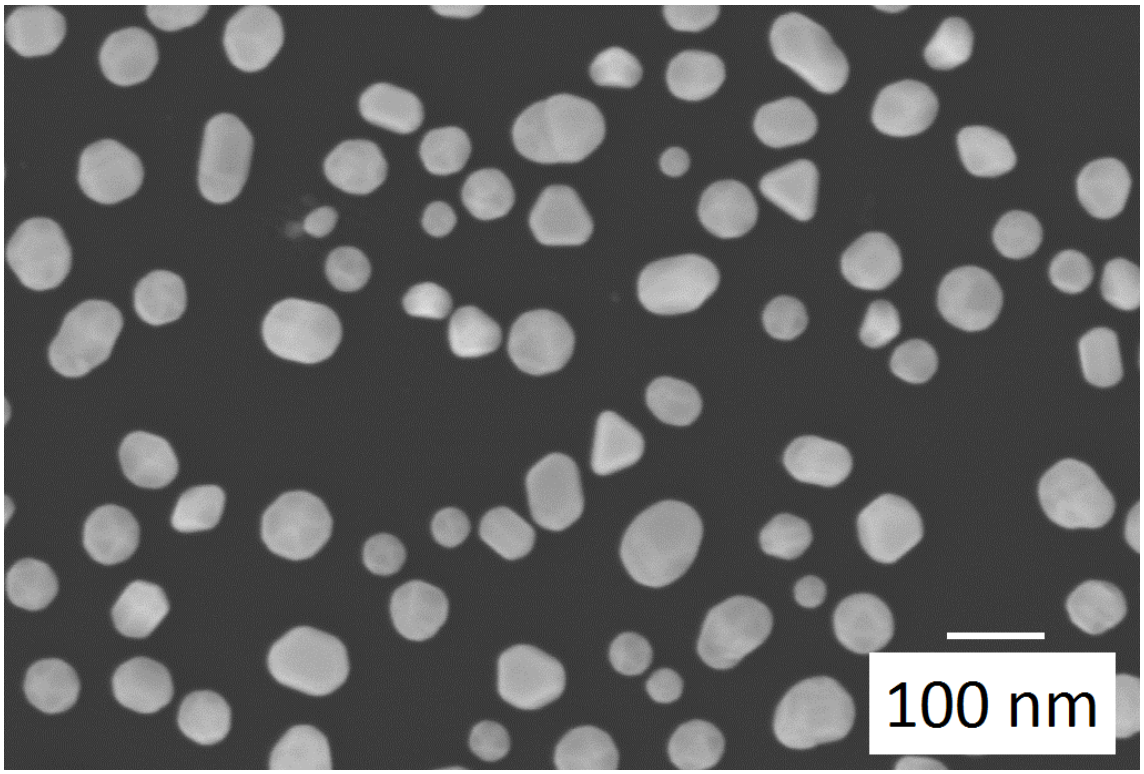

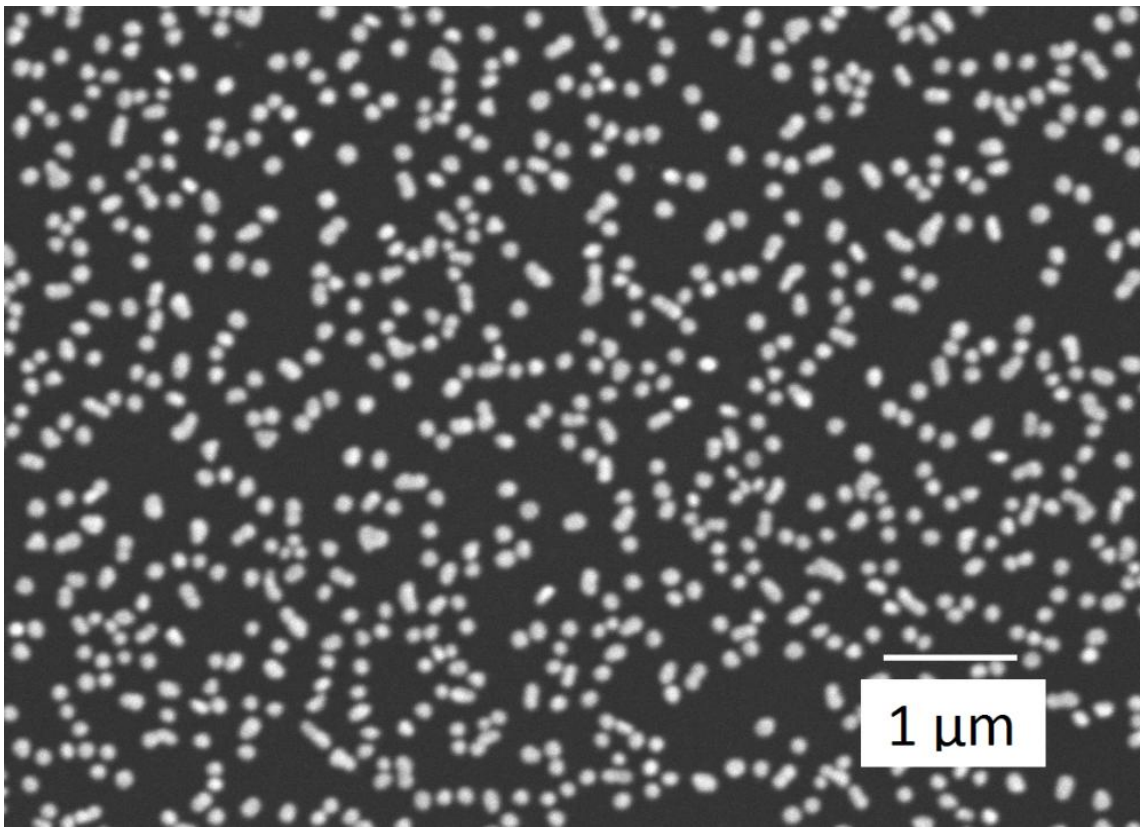

Figure 3

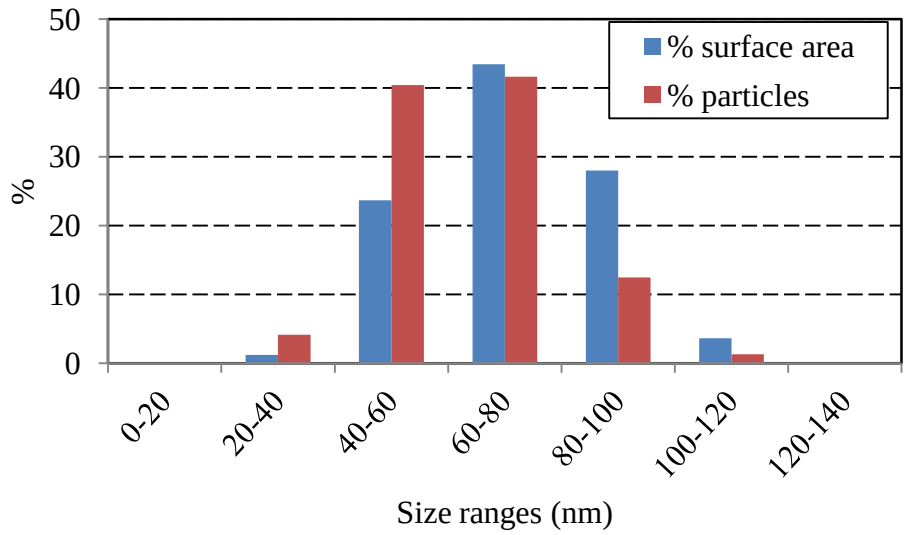
50
40
30
20
10
0
%
% surface area
% particles
0-20
20-40
40-60
60-80
80-100
100-120
120-140
Size ranges (nm)

Figure 4

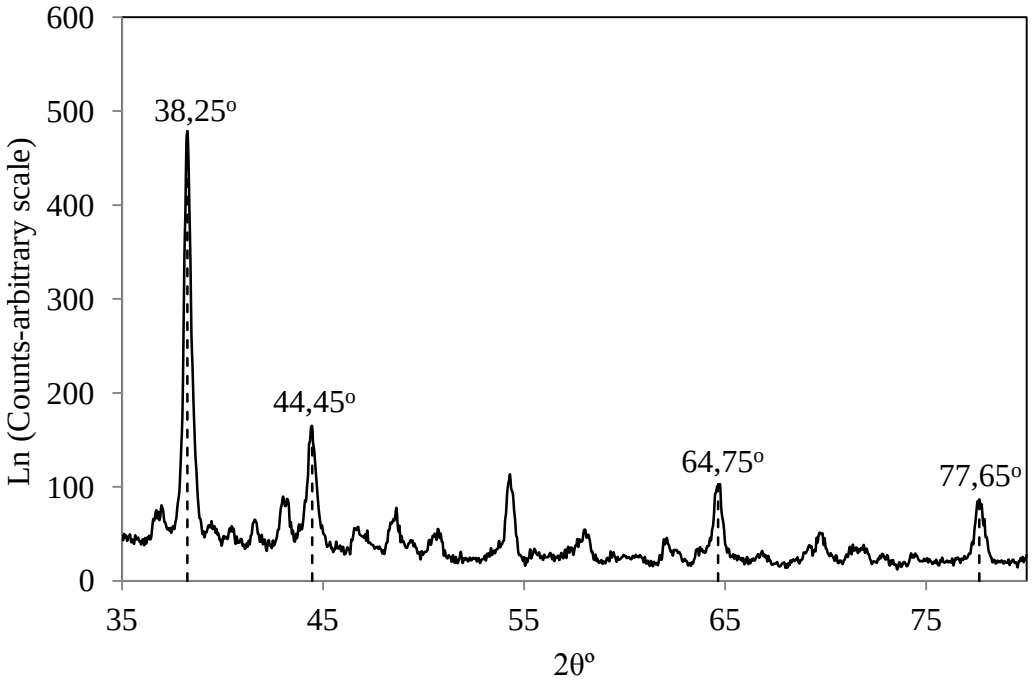
600
500
400
300
200
100
0
Ln (Counts-arbitrary scale)
38,25º
44,45º
64,75º
77,65º
35
45
55
65
75
2θº

Figure 5

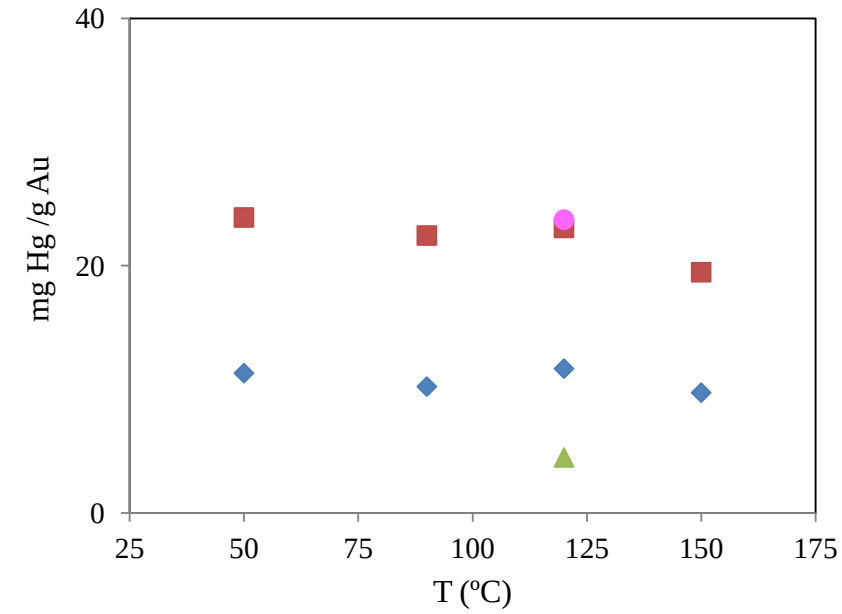
40
20
0
mg Hg /g Au
25
50
75
100
125
150
175
T (ºC)

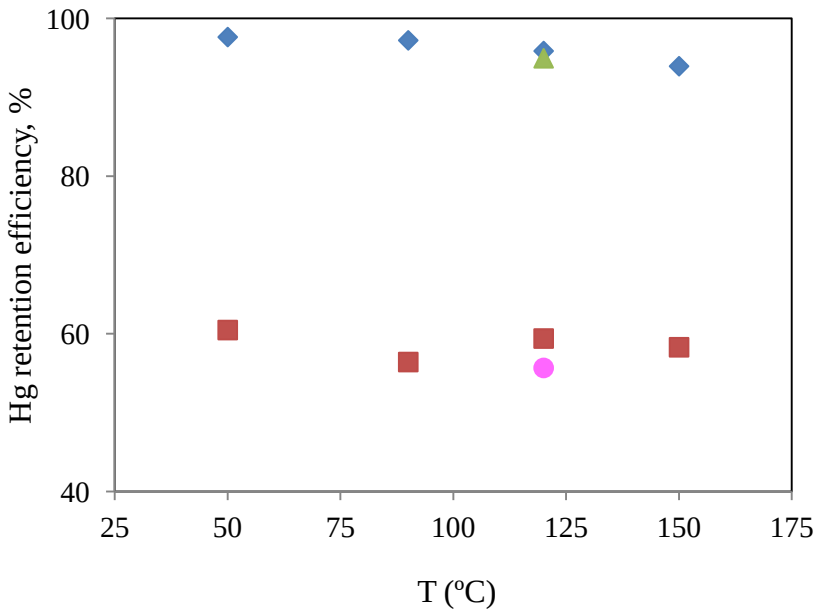
100
80
60
40
Hg retention efficiency, %
25
50
75
100
125
150
175
T (ºC)

Figure 6

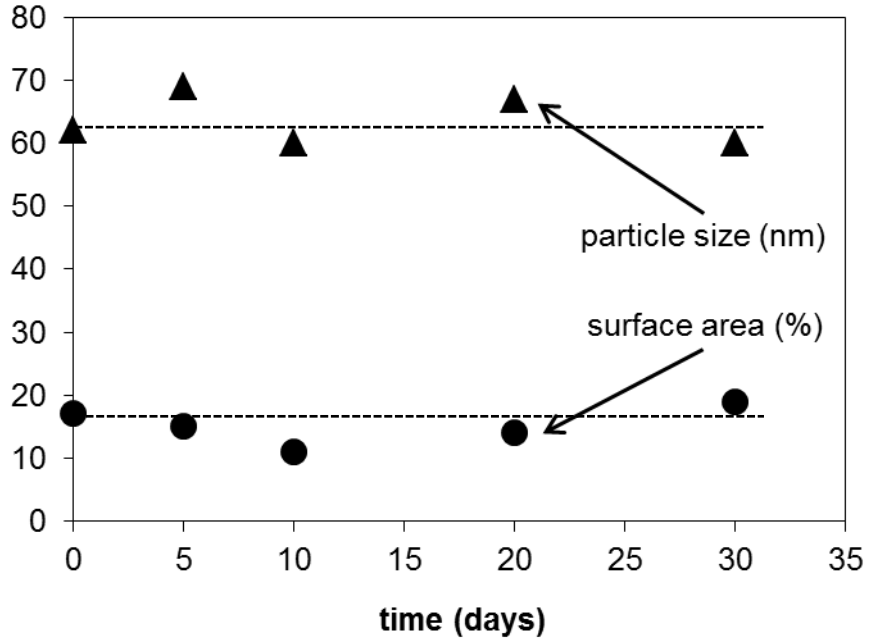
80
70
60
50
40
30
20
10
0
0
5
10
15
20
25
30
35
time (days)
particle size (nm)
surface area (%)

Figure 7

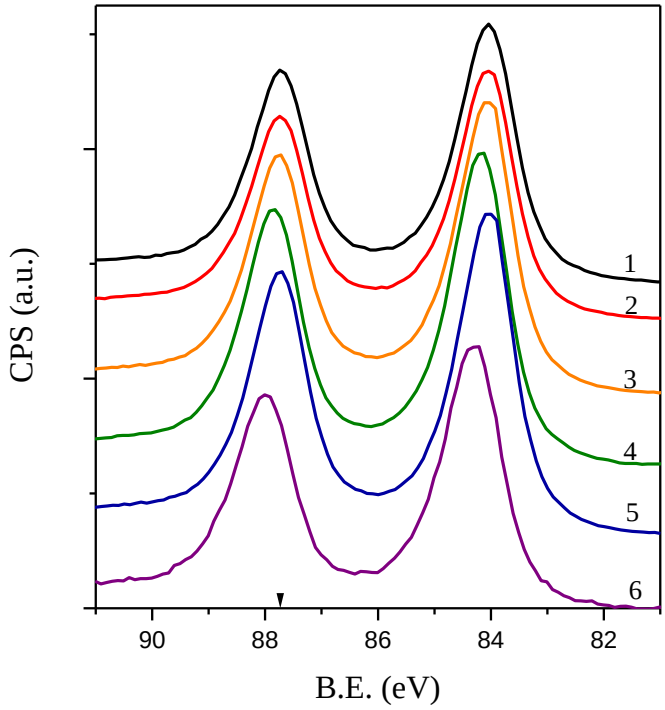

Figure 8

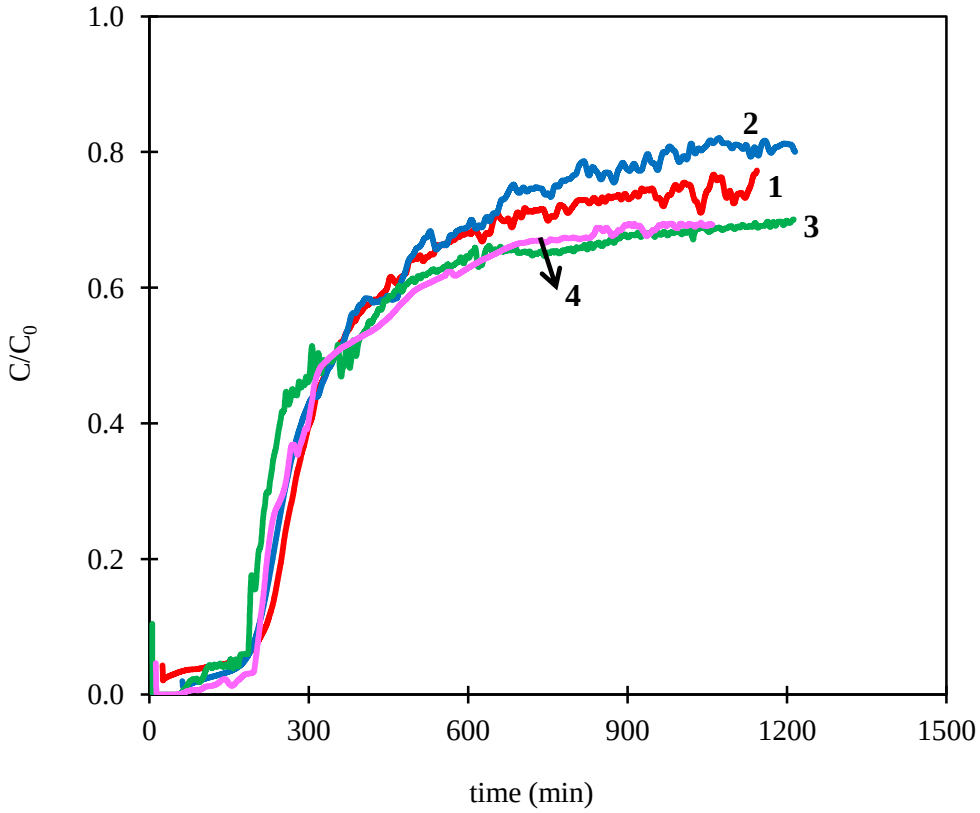

Figure 9